Aerothermodynamics of Transatmospheric Vehicles

Michael E. Tauber* and Gene P. Menees†
NASA Ames Research Center, Moffett Field, California
and
Henry G. Adelman†
Eloret Institute, Sunnyvale, California

A transatmospheric vehicle (TAV) using air-breathing propulsion requires a long acceleration period within the denser part of the atmosphere to reach orbital speed. The long flight time, coupled with the need for a low-drag configuration, results in the severe heating of parts of the vehicle. The ascent peak stagnation point and wing leading-edge equilibrium wall temperatures are about 3500 and 2600 K respectively, probably requiring some form of mass addition cooling. The corresponding temperatures during entry are 1000 K lower. The vehicle windward centerline temperatures are more moderate, with values peaking around 1300 K during both ascent and entry. Therefore, radiative cooling should be effective over large areas of the vehicle. The windward centerline heat loads during entry are comparable to those for low-acceleration ascent trajectories. However, the ascent heat loads for the stagnation point and wing leading edge are about three times higher than those during entry. For comparison, the entry heat load for the TAV's stagnation point is about three times higher than the value for the Shuttle. Therefore, the ascent heat load at the TAV's stagnation point exceeds the Shuttle's entry value by an order of magnitude.

Nomenclature

A = reference area of vehicle
a = acceleration
C = constant, Eq. (10)
C_D, C_L = drag and lift coefficients, respectively
D = drag
g = acceleration of gravity
g_w = ratio of wall enthalpy to total enthalpy
K = constant, Eq. (3b)
L = lift
m = vehicle mass
Q = total heat load per unit area
q = dynamic pressure
$\dot{q}$ = heat-transfer rate into the body per unit area
R_o = planetary radius
r_n = body nose radius
T = thrust
t = time
V = flight velocity
V_s = surface grazing (circular) satellite speed (7.9 km/s)
x = distance measured along body surface
Δ = wing leading-edge sweep angle
θ = bank angle
ϵ = surface emissivity
ρ = freestream density
ρ_o = sea-level atmospheric density
ϕ = local body angle with respect to freestream
σ = Stefan-Boltzmann constant

Subscripts

FP = flat plate
f = final value
i = initial value
L = laminar boundary layer (also 1)
LE = wing leading edge
max = maximum
o = stagnation point (also 2)
T = turbulent boundary layer
w = wall

Introduction

THE developing need for economical access to space and commercial global transportation has stimulated renewed interest in hypervelocity transatmospheric vehicles (TAV's). By providing short launch notice and turnaround times, such aerospace vehicles would have responsive, flexible operational characteristics approaching those of aircraft and would eventually replace the Shuttle. The TAV's would be able to take off and land from ordinary runways and operate in low-Earth orbits. A lower-speed variant of such a vehicle may be used to transport passengers or high-value cargoes to any location on the Earth in a small fraction of the flight time of current jet airliners.

The President's endorsement of funding for the development of a Space Station and a "transatmospheric vehicle" has led to the establishment of a National Aerospace Plane Program. These events, combined with the tremendous advances in enabling technology since the X-15 hypersonic airplane spearheaded the nation's high-altitude flight program a generation ago, have propelled an operational aerospace plane from a fantasy to a national technological goal by the twenty-first century.

The missions proposed for the aerospace plane would use primarily air-breathing propulsion systems for extended periods of hypervelocity flight up to orbital speed within the atmosphere. These conditions subject the vehicle to severe local heat fluxes and total heat loads, which determine the thermal protection requirements and are a major factor in the vehicle's design. The present paper contains a parametric analysis of the aerothermodynamic environment encountered

Presented as Paper 86-1257 at the AIAA/ASME 4th Joint Thermophysics and Heat Transfer Conference, Boston, MA, June 2-4, 1986; received July 21, 1986; revision received March 10, 1987.

*Research Scientist. Associate Fellow AIAA.
†Research Scientist. Member AIAA.

during both the ascent and re-entry phases of typical missions in support of future space activities.

Although finite-rate thermochemical relaxation phenomena may affect the shock-layer flow and heating at very high altitudes, all the present computations were made assuming that equilibrium flow conditions prevail, which is conservative. For the ascent, a family of representative trajectories are defined, and the surface heating and equilibrium wall temperatures are calculated at selected body locations on a baseline configuration. The re-entry flight paths are equilibrium glide trajectories; maximum heating rates and wall temperatures are obtained for the same body locations for the re-entry calculations as for the ascent calculations. Total heat loads are also obtained for these locations for both ascent and entry. The effects of boundary-layer transition phenomena are considered, and the impact of turbulent flow on the heating rates is evaluated. The prediction techniques were compared with Shuttle entry flight data, and good correlations were obtained.

Analysis

Rocket-launched space vehicles, such as the Shuttle orbiter, experience relatively little aerodynamic heating during launch. The large thrust available during ascent results in passage through the sensible atmosphere in a matter of minutes. Burnout velocity is reached at very high altitudes, where the aerodynamic heating is low. For instance, the time-integrated heating (total heat load) at the Shuttle orbiter nose stagnation point is almost two orders of magnitude less during launch than during atmospheric entry. In contrast, a vehicle using an air-breathing propulsion system must fly a long time in the denser portion of the atmosphere to develop sufficient thrust to accelerate to orbital speed. This extended period of hypervelocity atmospheric flight exposes the vehicle to high local heating rates and large total heating loads. To determine the thermal protection requirements for the TAV, it is, therefore, necessary to model the ascent flight paths, as well as the entry trajectories, to calculate the heating at selected body locations. This formulation will be performed in the following section.

A major objective is the development of relatively simple but realistic and adequately verified methods for calculating the convective aerodynamic heating during the high-speed flight of a TAV. A primary advantage of a simplified analysis is the short computing time. Short computing time permits the method to be applied to such tasks as parametric studies, conceptual vehicle design, and trajectory optimization, where many passes through the program may be required. Unlike other orbital vehicles, the TAV will experience severe aerodynamic heating during ascent as well as entry; therefore, computing-time economy is important for TAV parametric heating calculations.

Trajectories

For the ascent, a group of representative trajectories is defined. The objective is to determine flight paths that can be parametrically varied but are generally applicable for air-breathing power plants, without having to specify details such as engine cycles, efficiencies, and so on. For the atmospheric entry, the equilibrium glide trajectory[1] is stipulated. The equilibrium glide flight path is flown by manned vehicles that are returning from near-Earth orbit and that have adequate lift, since the path affords low decelerations.

Ascent

The entire trajectory consists of a number of segments beginning with takeoff, then a subsonic climb, acceleration through the high-drag transonic regime to supersonic speed, followed typically by a hypersonic climb to high altitude. From the standpoint of heating, only hypersonic flight is of major concern. It is assumed here that the hypersonic flight segment is a constant indicated airspeed climb. This segment is a fuel-efficient climb path typically flown by subsonic or supersonic jet aircraft[2] and corresponds to flight at a constant dynamic pressure, so that

$$\tfrac{1}{2}\rho V^2 = q \tag{1}$$

where q is constant. The equation of motion along the flight path is

$$\frac{m\mathrm{d}V}{\mathrm{d}t} = T - D \tag{2a}$$

where T is the engine thrust. After substituting Eq. (1) into Eq. (2a), the acceleration along the flight path becomes

$$\frac{\mathrm{d}V}{\mathrm{d}t} = \frac{T}{m} - q\frac{C_D A}{m} \tag{2b}$$

The thrust T can be a function of many factors, including the type of power plant, the flight speed, and the altitude. However, to make the present analysis as general as possible, it is assumed that $(T-D)/m$ is approximately constant, so that the climb occurs at a constant acceleration

$$\frac{\mathrm{d}V}{\mathrm{d}t} \doteq a \tag{2c}$$

Therefore, two parameters are available to vary the high-speed portion of the ascent trajectory. The first is the dynamic pressure, which determines the flight altitude. The second parameter is the average (constant) value of the acceleration, which defines the flight time.

Entry

The flight-path expression for the equilibrium glide path comes directly from equating the difference between the lift and weight to the centrifugal force:[1]

$$L - mg = -\frac{mV^2}{R_o} \tag{3a}$$

where $L = qAC_{Lo}\cos\theta$ and C_{Lo} is the lift coefficient at zero bank angle θ, and R_o is the Earth's radius. This equation gives

$$\frac{\rho V^2}{V_s^2 - V^2} = \frac{2}{R_o}\frac{m}{C_L A} = K \tag{3b}$$

where V_s is the circular satellite speed and the right-hand side can be considered constant during the high-speed portion of the entry if the bank angle does not vary much. (Banking the vehicle reduces the effective L/D, thus decreasing the entry time and the duration of the heating pulse.)

The flight-path expression, Eq. (3a), is given in its simplest form, which neglects the Earth's rotation and also assumes the changes in g and R to be negligible. The effect of these simplifying assumptions will subsequently be illustrated when a comparison with flight data is made.

Aerodynamic Heating

It is assumed that the heating rate per unit area can be written in the form

$$\dot{q} = \frac{\mathrm{d}q}{\mathrm{d}t} = C\rho^N V^M \tag{4}$$

where N, M, and C are assumed constant. The form of Eq. (4) applies in the flight regime where boundary-layer theory is valid. Equation (4) is a good approximation for both laminar[3,4] and turbulent[5] convection at a catalytic surface in

the absence of boundary-layer mass addition. The numerical values used in Eq. (4) are taken from Refs. 3 and 5 and are for the stagnation point and turbulent flat-plate heating, respectively. The laminar flat-plate heating expression is a slightly simplified version of the relation derived in Ref. 4. None of the constants in Eq. (4) were modified using Shuttle or other flight data. (The values of N, M, and C are listed in the Appendix.) Assuming a fully catalytic wall is usually conservative, which makes Eq. (4) independent of the choice of heat shielding material. Since C is a weak function of the wall temperature, however, given by

$$T_w = (\dot{q}/\epsilon\sigma)^{1/4} \tag{5}$$

it is necessary to iterate between Eqs. (4) and (5) to find the heating rate.

The form of Eq. (4) is suitable for calculating the stagnation point or the flat-plate heat transfer. The wing leading-edge heating was computed using the swept-cylinder theory[6] in the form

$$\dot{q}_{LE} = [\tfrac{1}{2}(\dot{q}_o)^2 \cos^2\Delta + (\dot{q}_{FP})^2 \sin^2\Delta]^{1/2} \tag{6}$$

where Δ is the leading-edge sweep angle.

The beginning of boundary-layer transition from laminar to turbulent flow is predicted using a modified correlation of the local length Reynolds number and local Mach number.[7] The original correlation for cones, shown in Ref. 7, was modified and extended to nonaxisymmetric bodies by adding transition data from Shuttle flights.[8,9] The length of the transitional boundary-layer region is assumed to be the same as the preceding laminar flow distance. A linear variation is assumed between the laminar values and the fully established turbulent heating rates. Comparisons of laminar, transitional, and turbulent heating rates with Shuttle flight data will be presented later in this paper. Next, expressions for the heating rates and total heat loads during ascent and entry will be formulated.

Ascent

The heating rate per unit area during the hypersonic climb at a constant dynamic pressure is found by substituting Eq. (1) into Eq. (4):

$$\dot{q} = C(2q)^N V^{M-2N} \tag{7}$$

where q is the dynamic pressure. The total heat load per unit area is determined by integrating Eq. (7) using Eq. (2c):

$$Q = \frac{1}{a}\int_{V_1}^{V_2} C(2q)^N V^{M-2N}\,dV \tag{8}$$

Both the dynamic-pressure term and C are functions of velocity; the first is because N changes if transition occurs, while the second is weakly dependent on total enthalpy.

Entry

The heating rate per unit area during entry is determined by combining Eq. (3b) with Eq. (4):

$$\dot{q} = CK^N (V_s^2 - V^2)^N V^{M-2} \tag{9}$$

The peak heating rate occurs at[10]

$$V = \left(\frac{M-2N}{M}\right)^{1/2} V_s \tag{10a}$$

and

$$\rho = \left(\frac{2N}{M-2N}\right) K \tag{10b}$$

The expression for the peak heating rate is[10]

$$\dot{q}_{\max} = C(2NK)^N (V_s/\sqrt{M})^M (M-2N)^{M/2-N} \tag{11a}$$

or, in terms of vehicle parameters only,

$$\dot{q}_{\max} \sim \left(\frac{m}{C_L A}\right)^N \tag{11b}$$

The general expression for the total heat load per unit area is[10]

$$Q = \frac{2m}{C_D A}\int_{V_f}^{V_i} CK^{N-1}(V_s^2 - V^2)^{N-1} V^{M-2N}\,dV \tag{12}$$

In regions of the vehicle that experience only laminar heating, such as the stagnation point, the total heating is approximately

$$Q \approx C_1 K^{-1/2} V_s^2 \frac{m}{C_D A} \tag{13a}$$

After substituting for K, this gives the proportionality

$$Q \sim \left(\frac{m}{C_D A}\frac{L}{D}\right)^{1/2} \tag{13b}$$

The following section contains some comparisons between Shuttle flight data and calculations using the previously derived equations.

Comparison with Flight Data

Data from Shuttle flights STS-1, STS-2, and STS-5 will be compared with calculated entry trajectory and heating rate values. Specifically, the trajectory of STS-5 will be compared with results from the simple equilibrium glide equation. Comparisons will also be made of heating rate data from the three flights with calculated values.

Entry Trajectory

The entry velocity/altitude history from Shuttle flight STS-5[11] is compared with values calculated using the equilibrium glide expression, Eq. (3b), in Fig. 1. The STS-5 entry was made in the direction of the Earth's rotation, resulting in an entry velocity of 7.45 km/s. The angle of attack was roughly constant, varying from about 41 deg at entry to 38 deg at 3km/s; the bank angles varied from about 64 to 48 deg over the same velocity range. In evaluating Eq. (3b), a constant value of $K/\rho_o = 2(10^{-4})$ was used, corresponding to $\alpha = 40$ deg and an average bank angle of about 55 deg, where ρ_o is the sea-level atmospheric density. The equilibrium glide expression agrees well with the Shuttle trajectory over much of the high-heating part of the flight path. At the lower-speed end, the difference is mainly due to the Shuttle's decreasing angle of attack, which is not accounted for in Eq. (3b). Near entry, the discrepancy results primarily from neglecting the planetary rotation and, to a lesser degree, from assuming the gravitational acceleration g and the radius R to be constant in Eq. (3a).

Entry Heating

Comparisons were made with the stagnation point maximum heating rate determined from temperature measurements during Shuttle flight STS-5.[11] According to Eq. (10a) using $N = 0.5$ and $M = 3$, the stagnation point maximum heating rate occurs at $V = 0.82V_s$. During the re-entry of STS-5, the stagnation point peak heating occurred at $V = 0.83V_s$. The stagnation point maximum heating rate using Eq. (11a) was 52.0 W/cm^2 for an effective nose radius of

89 cm. Using the exact flight conditions in Eq. (4) gave 44.7 W/cm^2. The peak heating rate shown in Ref. 11, calculated using the BLIMP code for a fully catalytic surface and equilibrium flow, was 45.4 W/cm^2. The difference between Eq. (11a) and the flight calculation of Ref. 11 was 15%. The actual peak heating rate during the flight was about 34 W/cm^2. Nonequilibrium flowfield effects and reduced wall recombination rates caused by the partially catalytic tiles may account for the lower heating rates.[11]

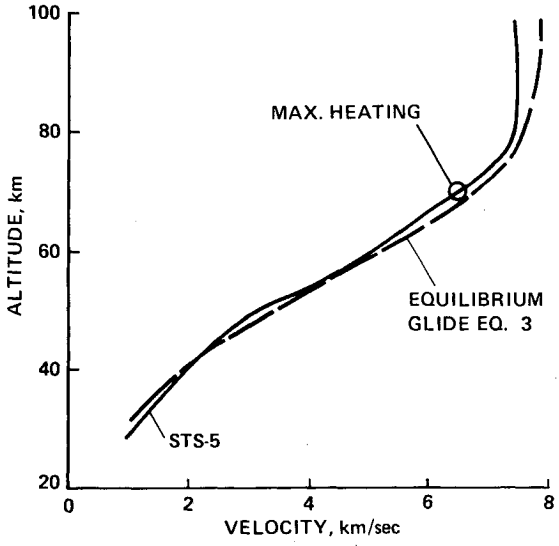

Fig. 1 Entry flight-paths comparison.

The STS-1 and STS-2 Shuttle flight centerline heating rates, again determined from temperature measurements,[8,12,13] are compared with calculations at six flight conditions in Fig. 2. The laminar and turbulent flat-plate versions of Eq. (4) were used (see Appendix). The STS-2 flight conditions shown in Fig. 2a cover the high-speed, high-altitude, laminar boundary-layer regime. The agreement between the measured and calculated heating rates is better over the forward portion of the vehicle than over the aft part, where the flight values are substantially higher and do not exhibit the $x^{-1/2}$ decrease with distance characteristic of an undisturbed laminar boundary layer. (Chemical nonequilibrium and reduced wall catalyticity may be responsible.[12,13]) However, at the lower speeds and altitudes where STS-1 measurements were made, the molecular dissociation was sufficiently small, or absent, to make catalytic wall effects negligible. Note that laminar, transitional, and turbulent boundary-layer heating are clearly evident in Fig. 2b. (The error bars represent uncertainties in the surface emissivity.[8]) The high-entropy gas layer generated by the Shuttle's blunt nose substantially increases the laminar heating near $X/L = 0.1$ at the flight conditions shown in Fig. 2b, where the flow should be in equilibrium. However, the much sharper nose of a TAV should largely eliminate the high-entropy layer, and the flat-plate approximation should yield more reasonable laminar heat-transfer values. The fully turbulent heating predictions are somewhat too high, which is typical for a method based on reference enthalpy. The comparisons shown in Fig. 2 cover an atmospheric density range of 300, while the flight speeds varied by a factor of 3.3. In view of the simplified nature of the present analysis, the overall agreement is good enough to meet the objectives of the parametric study.

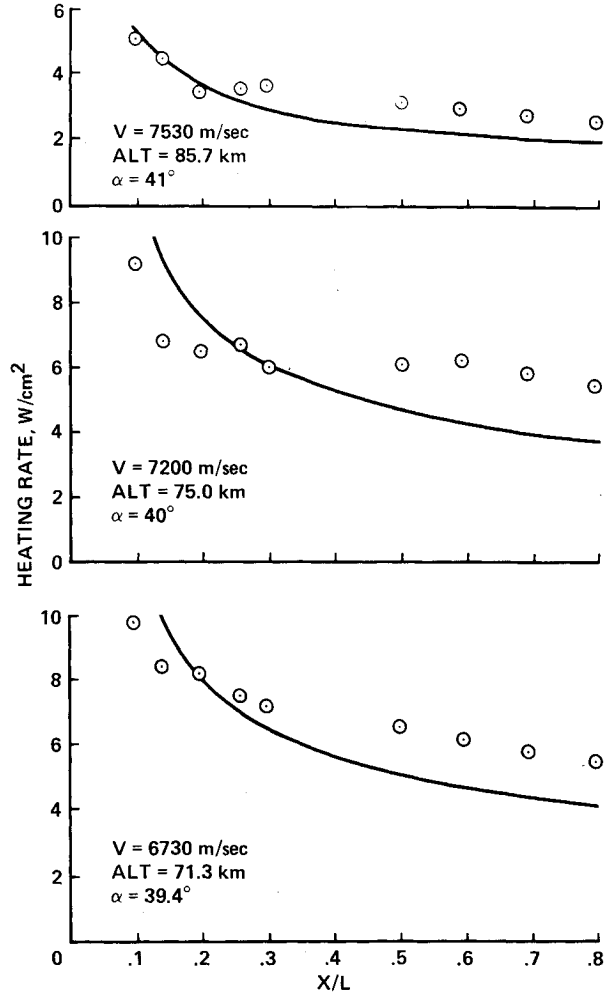

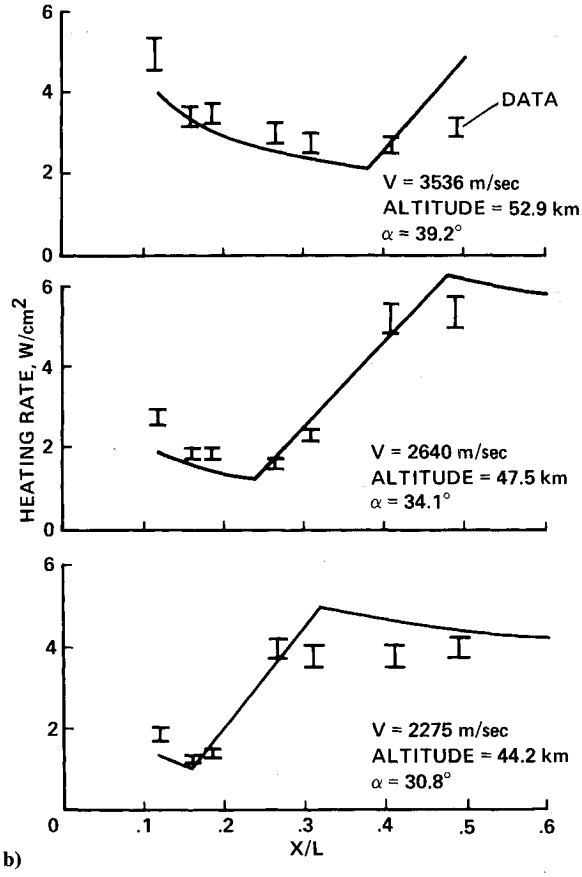

Fig. 2 Comparison of centerline heating calculations with flight data: a) STS-2, b) STS-1.

Study Parameters

It is desirable to make the study general, without defining a detailed vehicle configuration and specific missions. The ascent parameters studied consist of a family of hypersonic climb flight paths accelerating to a speed of 8 km/s. The vehicle could then coast to higher altitudes or out of the atmosphere; however, the coast phase is not analyzed here. Subsequently, the vehicle re-enters the atmosphere along one of a series of equilibrium glide trajectories, and the analysis is resumed.

Vehicle Characteristics

It is desirable to avoid using a specific vehicle configuration. However, the extended period of hypersonic flight required to achieve orbital velocity within the atmosphere mandates low-drag shapes.[14-16] These configurations should have substantially higher lift-to-drag ratios than the Shuttle. To reduce the number of parameters, the following geometric assumptions are made. The bottom surface of the vehicle is taken to be approximately flat, with an angle of incidence of +2 deg. The radius of the vehicle's nose is 10 cm. The wing leading edge is swept back at 75 deg and has a 5-cm radius at the location where heating is calculated. During the hypersonic part of the ascent, the angle of attack is assumed to be 3 deg. During the high-speed part of the entry, a 35-deg angle of attack is used.

Ascent Trajectories

The hypersonic part of the climb trajectories, when heating is large, is assumed to occur at constant dynamic pressures of 0.1, 0.2, and 0.4 atm [Eq. (7)]. The average accelerations during the climbs are assumed to be constant at values varying from 0.2 to 0.8 g [Eq. (8)].

Entry Trajectories

The entry trajectories and accompanying peak heating rates are direct functions of the parameter, m/C_LA [Eqs. (3b) and (11)]. The high-speed values of m/C_LA are varied from 200 to 800 kg/m^2. (The values of m/C_LA for the Shuttle are in the neighborhood of 700 kg/m^2 at high speeds.) The total heating load during entry depends on the group of terms $(m/C_DA \times L/D)$, as in Eqs. (12) and (13); the values of this parameter are varied from 400–1800 kg/m^2. In the next section, heating rates, equilibrium wall temperatures, and total heat loads during ascent and entry will be presented in a parametric manner.

Results

The parameters described are now used to calculate the heating rates, equilibrium wall temperatures (using $\epsilon = 0.8$), and total heating loads at the vehicle's stagnation point, at a representative location on the wing leading edge and over the forward portion of the bottom surface centerline. Heating at all three body locations will be illustrated for three ascent trajectories and three entry trajectories.

Ascent Heating

The three ascent flight paths are characterized by constant dynamic pressures of 0.1, 0.2, and 0.4 atm. The heating rate at the stagnation point and wing leading edge and the corresponding equilibrium wall temperatures are shown in Fig. 3 as a function of velocity. (The location of the leading-edge point is 10 m from the wing root measured along the leading edge.) The steep pressure gradients resulting from small radii of curvature (compared to the Shuttle, for instance) produce severe heating. The heating rates at the stagnation point range from 470 to 930 W/cm^2 at 8 km/s. The corresponding wall temperatures vary from about 3200 to 3800 K and are far beyond the radiative cooling capabilities of existing, nonablating, heat shield materials. Even the leading-edge point experiences heating rates of 120–320 W/cm^2, resulting

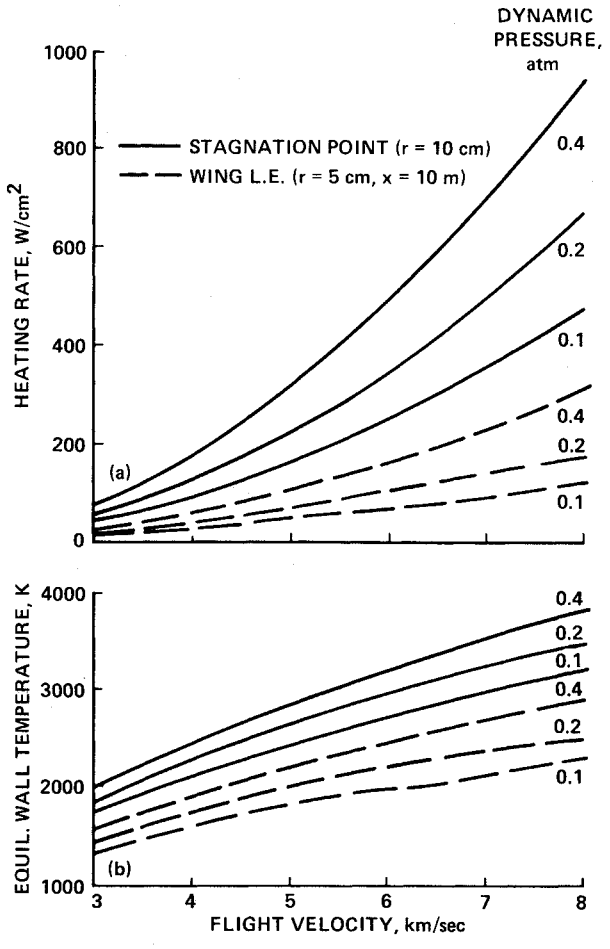

Fig. 3 Ascent heating.

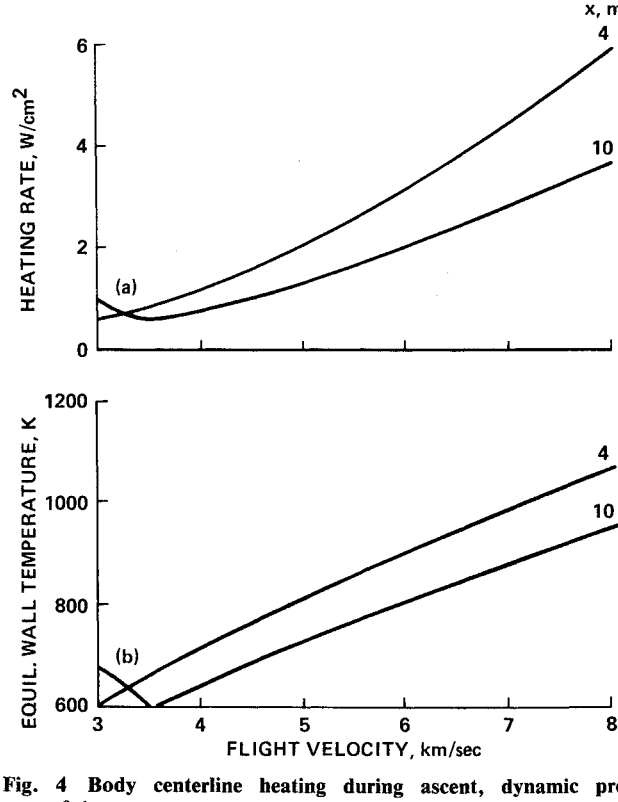

Fig. 4 Body centerline heating during ascent, dynamic pressure = 0.1 atm.

in wall temperatures of 2250–2900 K. Therefore, both the stagnation point region and the wing leading edge may require some form of active cooling such as ablation or transpiration. However, the areas of the vehicle requiring ablation or active cooling may be relatively small. This can be seen in Figs. 4–6, where the vehicle's centerline heating and temperatures are shown again at speeds up to 8 km/s and for all three trajectories at points 4 and 10 m from the nose. Despite strong turbulent heating at $q=0.4$ atm and $x=10$ m, the temperatures are below 1300 K, which is sufficiently low to permit radiative cooling. In fact, the temperatures are comparable to Shuttle windward centerline peak value during entry. (The relaminarization of the boundary layer that occurs for all three trajectories, but is most dramatic in Fig. 6, is due to the increasing boundary-layer edge Mach number with increasing speed.)

The total heating loads at the stagnation point and wing leading edge are shown in Fig. 7 as a function of average acceleration. As expected, the total heating declines dramatically with increasing acceleration, since the duration of the heating pulse decreases. In fact, the heating load is inversely proportional to the average acceleration [Eq. (8)], causing the stagnation point total heating to decrease from nearly 1.1. MJ/cm^2 at 0.2 g to about 280 kJ/cm^2 at 0.8 g. The leading-edge total heat loads are about one-quarter of the stagnation point values. The distributions of the centerline total heat loads are shown in Fig. 8 for an average acceleration of 0.2 g. [The heat loads for any other average acceleration can be easily calculated from the inverse ratio of the accelerations (Eq. (8).] Note that 10 m from the nose, the total heat load for the $q=0.4$ atm trajectory is twice as high as for the $q=0.2$ atm case. The disproportionately greater heating is due to the longer period of turbulent flow resulting from flight at higher dynamic pressure; this is made evident by comparing Figs. 5 and 6. In sharp contrast with

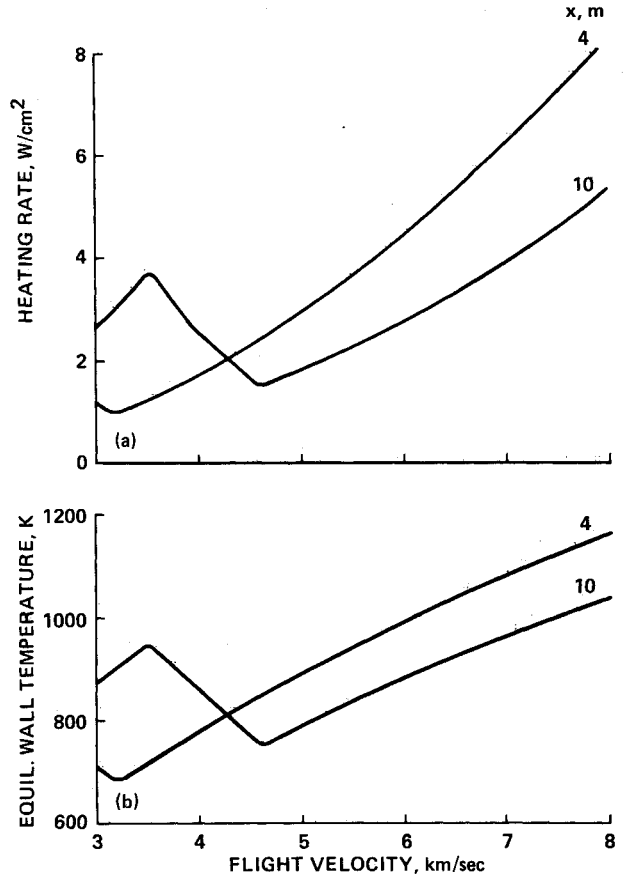

Fig. 5 Body centerline heating during ascent, dynamic pressure = 0.2 atm.

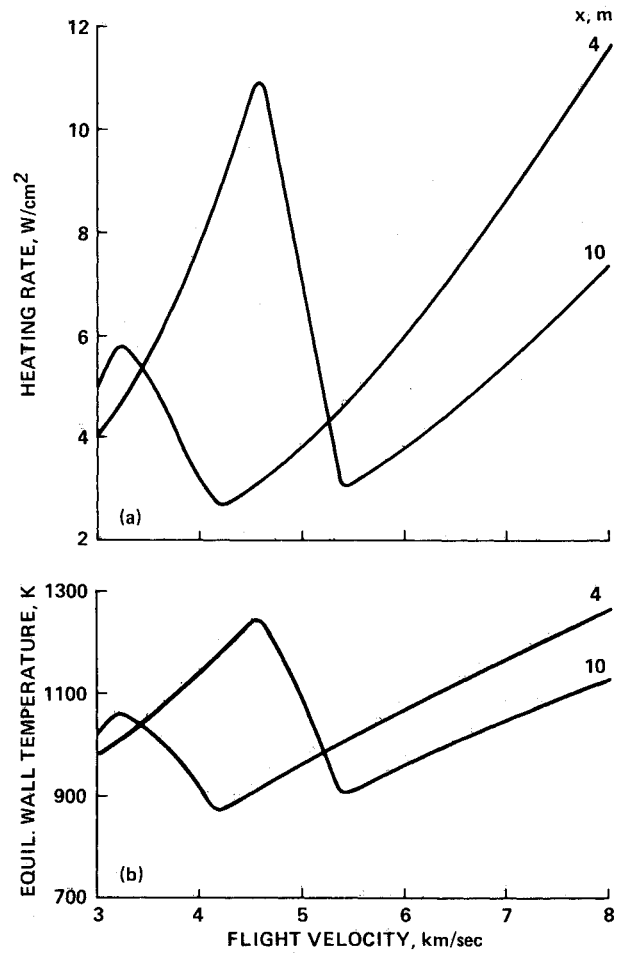

Fig. 6 Body centerline heating during ascent, dynamic pressure = 0.4 atm.

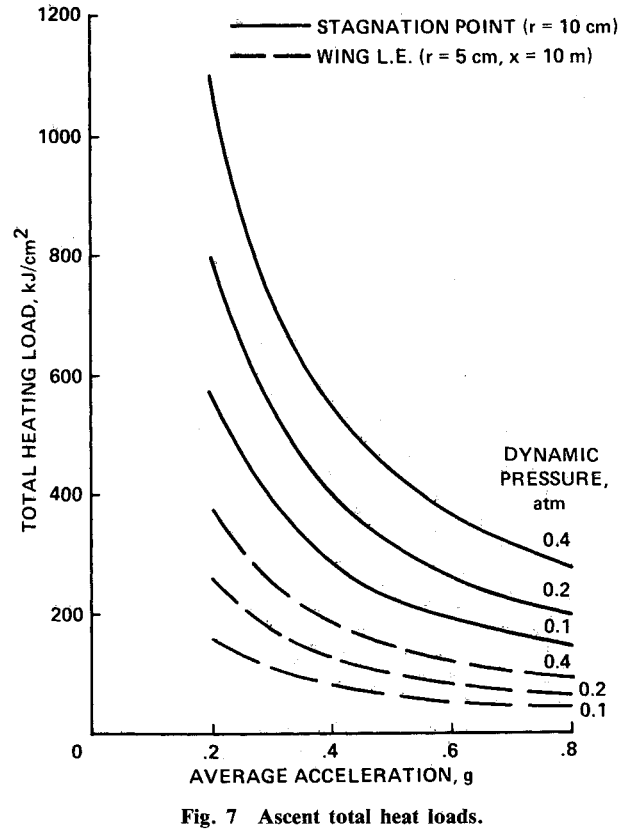

Fig. 7 Ascent total heat loads.

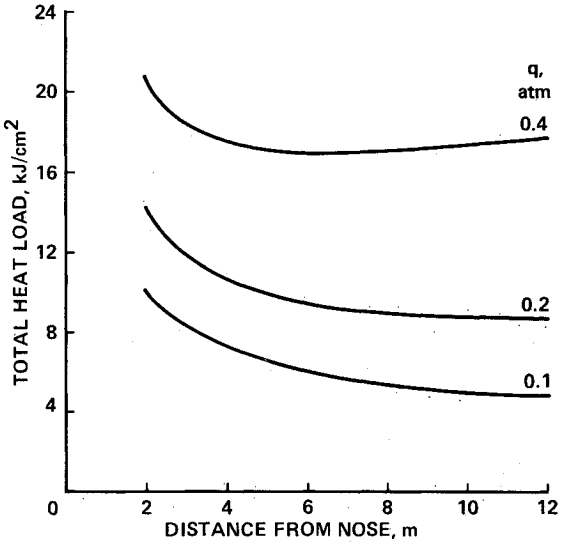

Fig. 8 Ascent total heat loads on centerline.

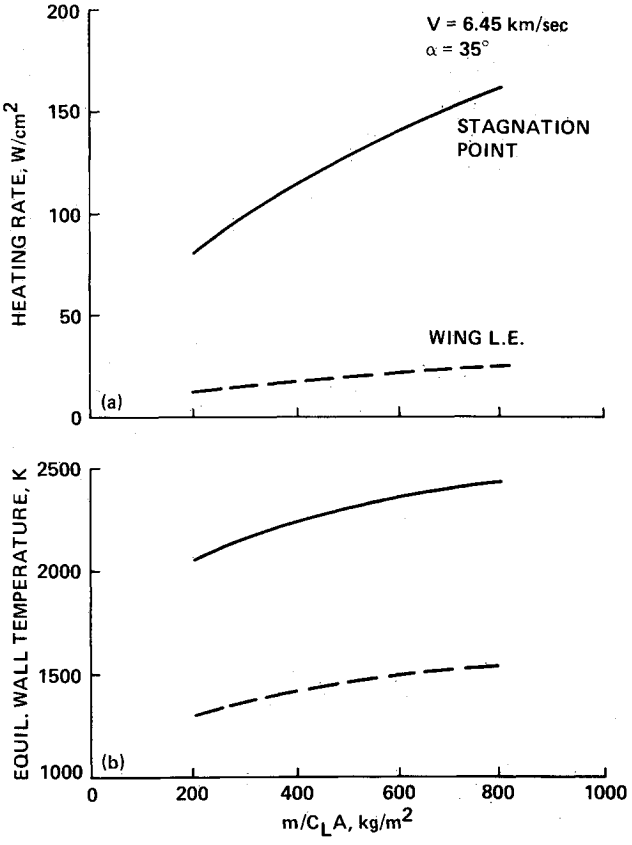

Fig. 9 Entry peak heating rates.

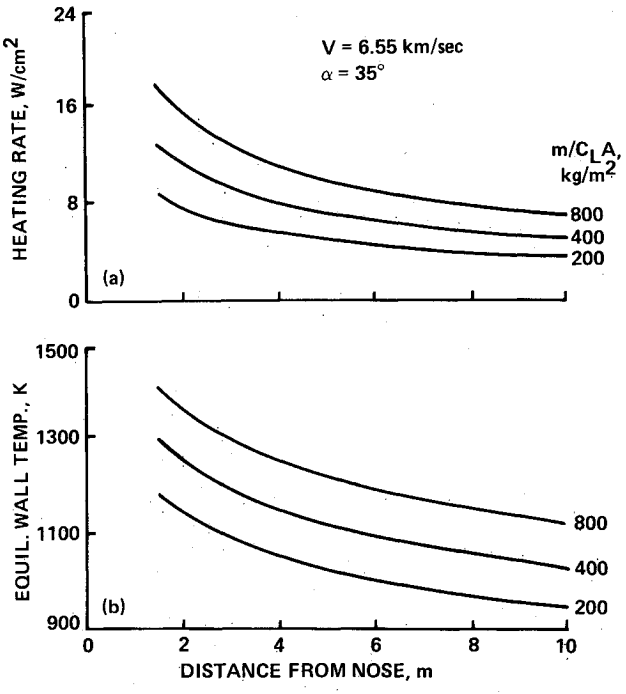

Fig. 10 Entry peak heating rate distribution on centerline.

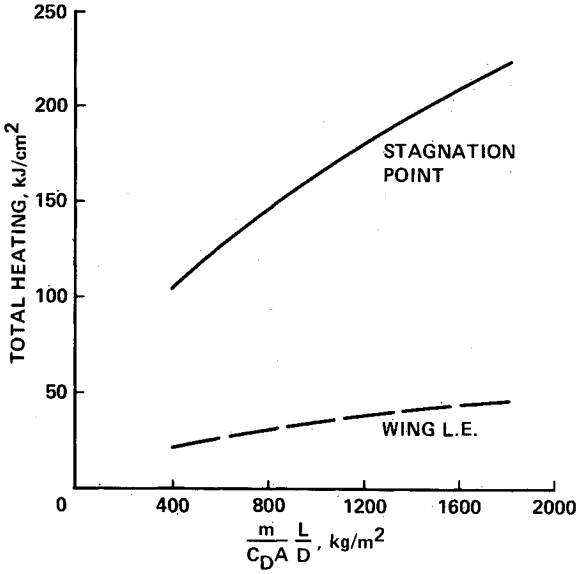

Fig. 11 Total heat loads during entry.

past experience, the heating environment encountered by the TAV upon atmospheric entry is usually more benign than that encountered during ascent.

Entry Heating

The peak entry heating rates at the stagnation point and wing leading edge are shown in Fig. 9, while Fig. 10 illustrates the centerline distributions. The conditions for the three entry trajectories, characterized by values of m/C_LA of 200, 400, and 800 kg/m^2, are illustrated. The stagnation point and leading-edge peak heating is nearly an order of magnitude less, and the temperatures are about 1000 K lower than the maximum values during ascent. However, the windward centerline peak heating is comparable to values encountered during ascent because of the high angle of attack during entry. As can be seen from Eq. (13b), high angles of attack increase the drag coefficient and decrease the lift/drag ratio, thus reducing the entry time and total heat load. The result can be seen in Fig. 11, where the total heat loads experienced by the stagnation point and the wing leading edge are shown. The vehicle centerline heat loads are presented in Fig. 12. Despite the high angle of attack, the centerline heat load is comparable to values encountered for a low-acceleration ascent trajectory. The entry heat pulse is shorter than the ascent pulse, and boundary-layer transition does not occur until the vehicle has decelerated to well below the peak heating speed.[8] The entry heat loads at the stagnation point and wing leading edge average about one-third of those experienced during ascent.

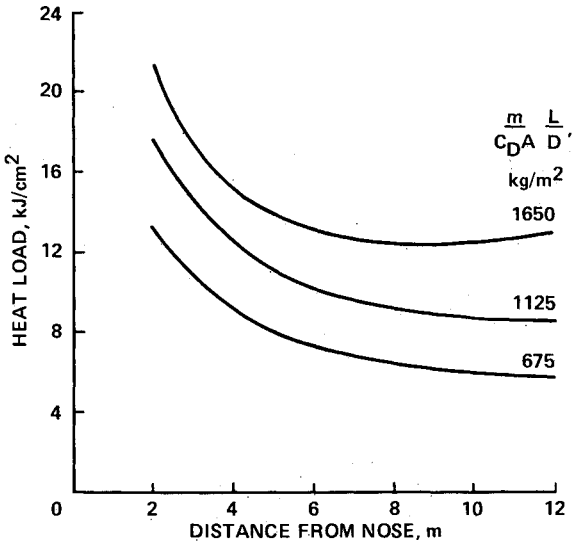

Fig. 12 Entry total heat loads on centerline.

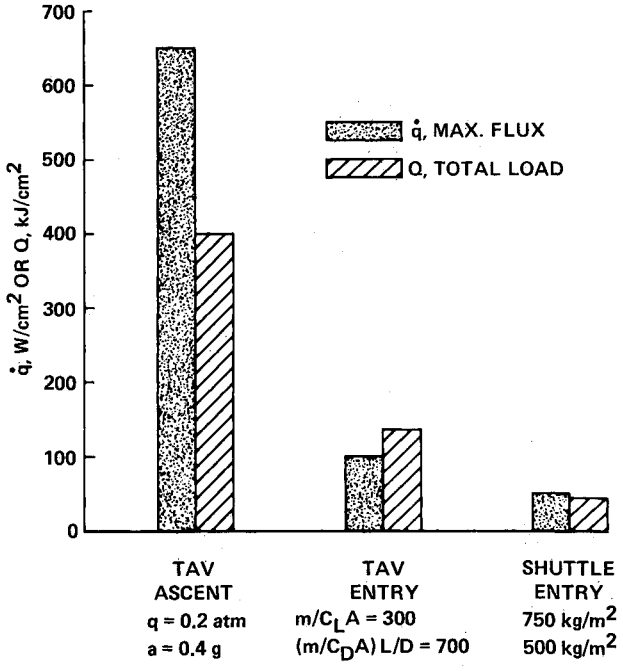

Fig. 13 Comparison of stagnation point heating.

The severity of the TAV heating environment is summarized in Fig. 13. In this figure, a comparison is presented between the TAV ascent and entry peak heating rates and total heat loads and the corresponding values for a typical Shuttle entry.[11] Note that the TAV's ascent peak heating rate is over an order of magnitude greater than the Shuttle's entry peak heating rate. At entry, the TAV's peak heating rate is still twice as high as the Shuttle's rate. The total heat load experienced during TAV ascent is almost an order of magnitude higher than for a representative Shuttle entry. The TAV's entry heat load is three times higher than that of the Shuttle. In contrast, the ascent heat load at the stagnation point of the rocket-launched Shuttle is less than 2% of the entry value[17] and too low to plot in Fig. 13.

Concluding Remarks

A TAV using primarily air-breathing propulsion must fly in the denser part of the atmosphere to achieve adequate acceleration to reach orbital speed. The elements of a very severe aerothermodynamic environment are, therefore, coupled with the requirement of low aerodynamic drag. To achieve low drag, the vehicle must be slender and have a relatively sharp nose and wing leading edges. The combination of the high heating rates experienced by surfaces with small curvatures and the long ascent times results in large total heat loads. Therefore, the most severe heating occurs during ascent at the stagnation point and wing leading edge. In contrast, atmospheric entry occurs at large angles of attack, since high drag is desirable to reduce the length of the heating pulse.

The ascent peak stagnation point and wing leading-edge equilibrium wall temperatures are about 3500 and 2600 K, respectively. Therefore, some form of mass addition cooling may be required for these regions of the vehicle. The corresponding temperatures during entry are 1000 K lower. The vehicle windward centerline temperatures are more moderate, however, with values peaking around 1300 K during both ascent and entry. Therefore, radiative cooling should be effective over large areas of the vehicle. The windward centerline heat loads during entry are comparable to those for low-acceleration ascent trajectories. However, the stagnation point and wing leading-edge ascent heat loads are about three times higher than those during entry. For comparison, the TAV stagnation point entry heat load is about three times higher than that of the Shuttle. The TAV's stagnation point ascent heating, therefore, exceeds the Shuttle entry value by an order of magnitude. The TAV thermal protection system design poses major challenges.

Appendix

The values of the constants in Eq. (4), for a fully catalytic surface, are listed here. The units of the heating rate are watts per square centimeter if the velocity is in meters per second and density in kilograms per cubic meter.

Stagnation point:

$$M=3,\ N=0.5,\ C=1.83(10^{-8})r_n^{-1/2}(1-g_w)$$

Laminar flat plate:

$$M=3.2,\quad n=0.5$$

$$C_1=2.53(10^{-9})(\cos\phi)^{1/2}(\sin\phi)x^{-1/2}(1-g_w)$$

Turbulent flat plate:

$$N=0.8$$

$$V\le 3962\ \text{m/s},\quad M=3.37$$

$$C_2=3.35(10^{-8})(\cos\phi)^{1.78}(\sin\phi)^{1.6}$$
$$\times x_T^{-1/5}(T_w/556)^{-1/4}(1-1.11g_w)$$

$$V>3962\ \text{m/s},\quad M=3.7$$

$$C_2=2.20(10^{-9})(\cos\phi)^{2.08}(\sin\phi)^{1.6}x_T^{-1/5}(1-1.11g_w)$$

References

[1]Eggers, A.J., Allen, H.J., and Neice, S.E., "A Comparative Analysis of the Performance of Long-Range Hypervelocity Vehicles," NACA TR-1382, 1958.

[2]Tauber, M.E. and Paterson, J.A., "Trajectory Module of the NASA Ames Research Center Aircraft Synthesis Program ACSYNT," NASA TM 78497, July 1978.

[3]Marvin, J.G. and Deiwert, G.S., "Convective Heat Transfer in Planetary Gases," NASA TR R-224, July 1965.

[4]Hanley, G.M., "Hypervelocity Laminar Convective Flat Plate Heating," *ARS Journal*, Vol. 32, Nov. 1963.
[5]Arthur, P.D., Shultz, H., and Guard, F.L., "Flat Plate Turbulent Heat Transfer at Hypervelocities," *Journal of Spacecraft and Rockets*, Oct. 1966, pp. 1549-1551.
[6]Rubesin, M.W., "The Effect of Boundary Layer Growth Along Swept-Wing Leading Edges," Vidya Corp. Rept. 4, 1958.
[7]Morkovin, M.V., "Critical Evaluation of Transition from Laminar to Turbulent Shear Layers with Emphasis on Hypersonically Traveling Bodies," AFFDL-TR-68-149, March 1969.
[8]Throckmorton, D.A., "Benchmark Aerodynamic Heat Transfer Data from the First Flight of the Space Shuttle Orbiter," AIAA Paper 82-0003, Jan. 1982.
[9]Goodrich, W.D., Derry, S.M., and Bertin, J.J., "Shuttle Orbiter Boundary Layer Transition at Flight and Wind Tunnel Conditions," *Shuttle Performance: Lessons Learned*, NASA CP 2283, 1983.
[10]Tauber, M.E., "Scaling Relations for Heating During Gliding Entry at Parabolic Speed," *AIAA Journal*, Dec. 1986, pp. 2047-2049.
[11]Curry, D.M., Rochelle, W.C., Chao, D.C., and Ting, P.C., "Space Shuttle Orbiter Nose Cap Thermal Analysis," AIAA Paper 86-0388, Jan. 1986.
[12]Shinn, J.L., Moss, J.N., and Simmonds, A.L., "Viscous Shock-Layer Heating Analysis for the Shuttle Windward Plane with Surface Finite Catalytic Recombination Rates," AIAA Paper 82-0842, June 1982.
[13]Kim, M.D., Swaminathan, S., and Lewis, C.D., "Viscous Shock-Layer Predictions of Three-Dimensional Nonequilibrium Flows Past the Space Shuttle at High Angle of Attack," *Shuttle Performance: Lessons Learned*, NASA CP 2283, March 1983.
[14]"British Study Space Shuttle Competitor," *Aviation Week and Space Technology*, Sept. 1984.
[15]Covault, C., "Advanced Space Transport Research Emphasis Growing," *Aviation Week and Space Technology*, Sept. 1985.
[16]Greeley, B.M. Jr., "U.S. Moves Toward Aerospace Plane Program," *Aviation Week and Space Technology*, Dec. 1985.
[17]Foster, L.D., Greenwood, T.F., and Lee, D.B., "Shuttle System Ascent Aerodynamic and Plume Heating," *Shuttle Performance: Lessons Learned*, NASA CP 2283, March 1983.